

1 **An Intertropical Convergence Zone shift controlled the terrestrial material supply on the Ninetyeast Ridge**

2 *Xudong Xu<sup>1,3,4</sup>, Jianguo Liu<sup>1,2,4,\*</sup>, Yun Huang<sup>1,\*</sup>, Lanlan Zhang<sup>1,4</sup>, Liang Yi<sup>2,5</sup>, Shengfa Liu<sup>2,6</sup>, Yiping Yang<sup>1,4</sup>, Li Cao<sup>1,3,4</sup>,*

3 *Long Tan<sup>1,3,4</sup>*

4 <sup>1</sup>Key Laboratory of Ocean and Marginal Sea Geology, South China Sea Institute of Oceanology, Chinese Academy of  
5 Sciences, Guangzhou 510301, China

6 <sup>2</sup>Laboratory for Marine Geology, Pilot National Laboratory for Marine Science and Technology, Qingdao 266061, China

7 <sup>3</sup>University of Chinese Academy of Science, Beijing 100049, China

8 <sup>4</sup>Southern Marine Science and Engineering Guangdong Laboratory (Guangzhou), Guangzhou 511458, China

9 <sup>5</sup>State Key Laboratory of Marine Geology, Tongji University, Shanghai 200092, China

10 <sup>6</sup>Key Laboratory of Marine Geology and Metallogeny, First Institute of Oceanography, Ministry of Natural Resources,  
11 Qingdao 266061, China

12 Corresponding authors: Jianguo Liu ([jgliu@scsio.ac.cn](mailto:jgliu@scsio.ac.cn)) and Yun Huang ([huangyun@scsio.ac.cn](mailto:huangyun@scsio.ac.cn))

13 **Abstract**

14 Among various climate drivers, direct evidence for the Intertropical Convergence Zone (ITCZ) control of sediment supply  
15 on the millennial scale is lacking, and the changes in ITCZ migration demonstrated in paleoclimate records need to be  
16 better investigated. Here, we use clay minerals and Sr-Nd isotopes obtained from a gravity core on the Ninetyeast Ridge  
17 to track the corresponding source variations and analyze the relationship between terrestrial material supply and climatic  
18 changes. On the glacial-interglacial scale, chemical weathering weakened during the North Atlantic cold climate periods  
19 and falling sea level hindered the transport of smectite into the study area due to the exposure of Andaman and Nicobar  
20 Islands. However, the influence of the South Asian monsoon on the sediment supply was not obvious on the millennial  
21 scale. We suggest that the north-south migration of the ITCZ controlled the rainfall in Myanmar and further directly  
22 determined the supply of clay minerals on the millennium scale because the transport of smectite was highly connected

23 with the ITCZ location; thus, the regional shift of the ITCZ induced an abnormal increase in the smectite percentage during  
24 the late Last Glacial Maximum (LGM) in our records. The smectite percentage in the studied core is similar to distinct  
25 ITCZ records but different in some periods, revealing that regional changes in the ITCZ were significantly obvious and  
26 that the ITCZ is not a simple north-south displacement and closer connections occurred between the Northern-Southern  
27 Hemispheres in the eastern Indian Ocean during the late LGM.

## 28 **1. Introduction**

29 Deposited sediments are essential recorders of the paleoclimate and paleoceanographic conditions since the climate is tied  
30 to the whole sedimentation process from weathering and transport to the deposition of sediments on land. The terrestrial  
31 materials of "source-sink" systems are supplied to marine environments under the combined effects of multiple climate-  
32 related driving forces and ocean processes (Li et al., 2018; Yu et al., 2019), and understanding these effects is crucial for  
33 reconstructing the coevolutionary relationship of the palaeoenvironment with the palae-ocean and palaeoclimate. Various  
34 factors may control the formation and transport of terrestrial materials at low latitudes, such as the northeastern Indian  
35 Ocean. Recently, the South Asian monsoon has been revealed to be the main driving force of terrestrial material supply in  
36 Bangladesh and of hydrological changes in the Bay of Bengal (BoB, Dutt et al., 2015; Gebregiorgis et al., 2016; Jousain  
37 et al., 2017; Li et al., 2018; Liu et al., 2021). Moreover, the Intertropical Convergence Zone (ITCZ) is an important climate-  
38 driving force in low-latitude regions (Deplazes et al., 2013; Ayliffe et al., 2013), which has a pivotal role in heat  
39 transportation on Earth (Schneider et al., 2014), and the north-south shift of the ITCZ is thought to connect the climates in  
40 the Northern and Southern Hemispheres (Huang et al., 2019; Zhuravleva et al., 2021). Because monsoon dynamics are  
41 shaped by large-scale meridional temperature gradients and an ITCZ shift in tropical monsoon areas (Mohtadi et al., 2016),  
42 there are hopeful opportunities to analyze sediment responses to ITCZ or monsoon variations. The paleoclimate  
43 breakthroughs mentioned above enable us to analyze the response of sedimentary records to the ITCZ shift in the BoB  
44 more accurately. However, evidence for direct control of terrestrial sediment supply by the ITCZ remains lacking, which

45 is an obstacle to understanding the response of the depositional environment to the ITCZ shift.

46 As the main deposition area for vast amounts of weathered Himalayan materials, the BoB accumulates numerous  
47 Himalayan terrestrial materials that are loaded by the Ganges-Brahmaputra (G-B) River (Goodbred and Kuehl, 2000) and  
48 forms the largest subaqueous fan, the Bengal Fan (3000 km long from north to south, 1400 km wide from east to west,  
49 with an area of  $3.9 \times 10^5$  km<sup>2</sup>; Curray et al., 2003). The eastern and western sides of the BoB correspond to the Andaman  
50 Sea and the Indian Peninsula, respectively, and the BoB is a natural site that is useful for studying the interactions between  
51 weathering and climatic factors since both sides of the bay are affected by the South Asian monsoon (Ali et al., 2015).  
52 Previous studies suggest that Himalayan material transported by the G-B River was the predominant source of material in  
53 the northern BoB (Li et al., 2018; Ye et al., 2020), and the main sources in the west BoB are the Indian Peninsula and  
54 Himalayan weathered material (Kessarkar et al., 2005; Tripathy et al., 2011; Tripathy et al., 2014). In the eastern BoB, the  
55 sediment source areas include the Himalayan (transported by the G-B river), Indo-Burman Ranges and the Myanmar region  
56 through which the Irrawaddy River flows (Colin et al., 1999; Joussain et al., 2016). The terrigenous detrital material in the  
57 Andaman Sea is mainly Myanmar-origin sediments transported by the Irrawaddy River (Ali et al., 2015; Awasthi et al.,  
58 2014; Colin et al., 2006). A series of terrigenous sediment issues, such as changes in the source area and proportion of  
59 terrigenous matter in various regions of the BoB from the LGM to the Holocene, the distribution range of terrigenous  
60 materials in the western and eastern BoB, and how the G-B River sediments are transported in the BoB, are unclear until  
61 now. Little attention has been given to sediment provenance in the southern BoB or, particularly, to the correlation of these  
62 sediment sources with climatic driving factors.

63 Recent studies have revealed that clay minerals can be used to effectively track changes in source areas in the source-  
64 sink system of the BoB due to the great differences in clay mineral components among the source areas around the BoB  
65 (Joussain et al., 2016; Li et al., 2017; Liu et al., 2019; Ye et al., 2020). Moreover, Sr-Nd isotopes have been widely reported  
66 to track the variations in sediment provenance in the BoB (Ahmad et al., 2005; Colin et al., 1999; Colin et al., 2006).

67 In this study, we measured clay minerals and Sr-Nd isotopes in a deep-sea gravity core obtained from the southeastern  
68 BoB (Figure 1) to reconstruct variations in the sources of sediments in the Ninetyeast Ridge and to further explore the  
69 climate forces that affected the supply of terrestrial materials during the past 45 ka. Core 171106 located above the abyssal  
70 plain at ~900 m, exempting from the influence of large-scale turbidite activities and receiving only fine-grained pelagic  
71 sediments that can reflect the changes in the provenance of the surrounding source area (Figure 1), which makes the  
72 terrestrial sediments on the Ninetyeast Ridge suitable for exploring the relationship between the paleoclimate and  
73 paleoenvironment in the BoB. Here, we aim to disentangle the ITCZ variability signal in marine sediments from multiple  
74 driving forces and further understand the response of sedimentary records to ITCZ migrations.

## 75 **2. Materials and methods**

### 76 **2.1. Chronology**

77 Gravity core 171106 (90.0040°E, 6.2105°N, water depth 2928 m) was collected by the *R/V Shiyan 1* vessel belonging to  
78 the South China Sea Institute of Oceanology (SCSIO), Chinese Academy of Sciences (CAS), from the Ninetyeast Ridge,  
79 northeast of the Indian Ocean (Figure 1). This core has a total length of 162 cm and consists of gray to green silty clays  
80 subsampled at 1-cm intervals. The age model of core 171106 was reconstructed based on 10 accelerator mass spectrometry  
81 (AMS) <sup>14</sup>C dates and Bayesian interpolations between these dates (Figure 2 and Table 1). AMS <sup>14</sup>C dating was performed  
82 on mixed planktonic foraminifera at Beta Analytic Inc. More than 20 mg of intact mixed planktonic foraminifera shells  
83 were selected from the >150 μm fractions of each sample (10 g dried sample). All radiocarbon ages were converted and  
84 reported as calendar years before present with the Calib8.2 software program with the Marine20 calibration dataset (Reimer  
85 et al., 2020). A continuous depth-age model was performed using Bacon software by dividing a sedimentary sequence into  
86 many thin segments and estimating a linear accumulation rate for each segment based on the calibrated <sup>14</sup>C dates and a  
87 Bayesian approach (Blaauw and Christen, 2011).

## 88 2.2. Clay mineralogy

89 Clay minerals (<2  $\mu\text{m}$ ) were separated from the sediment samples by sedimentation according to Stokes' settling velocity  
90 principle after organic materials and carbonates were removed with 15% hydrogen peroxide ( $\text{H}_2\text{O}_2$ ) and 0.1 N hydrochloric  
91 acid (HCl), respectively. We used the sedimentation method by placing the sample in glassware with an inner diameter of  
92 7 cm and a height of 10 cm at an experimental temperature of 19 °C. The sedimentation time was calculated as 4 hours and  
93 10 minutes according to Stokes' formula. The upper 5 cm of liquid was extracted, followed by centrifugation at 4800 rpm  
94 for 10 minutes, and the smear was made into a natural slice. The natural slice was heated in an oven at 60 °C for 24 hours  
95 to make ethylene glycol saturated slides for the subsequent test. The clay mineral slides were measured using routine X-  
96 ray diffraction (XRD) equipment (Bruker Inc, D8 ADVANCE) in the Key Laboratory of Ocean and Marginal Sea Geology,  
97 SCSIO, CAS. Clay mineral abundance was calculated by measuring the peak areas of smectite (15-17 Å), illite (10 Å) and  
98 kaolinite/chlorite (7 Å). Relative proportions of kaolinite and chlorite were calculated from the ratio of 3.57 Å/3.54 Å peak  
99 areas. The relative percentages of the four main clay minerals were estimated by calculating the integrated peak areas of  
100 characteristic basal reflections using Topas5P software with the empirical factors by [Biscaye \(1965\)](#). The reproducibility  
101 error of this method is  $\pm$  5-10%.

## 102 2.3 Sr-Nd isotope analyses

103 Twenty-two samples (<63  $\mu\text{m}$ ) from core 171106 were selected for isotope analyses, and we used the experimental method  
104 described by [Dou et al. \(2016\)](#). Carbonates were removed from 70 to 100 mg powdered bulk samples by leaching with  
105 0.25 N HCl for 24 h at 50 °C. The residues were then completely digested in high-pressure Teflon bombs using a HCl +  
106  $\text{HNO}_3$  +  $\text{HClO}_4$  + HF solution. Rb and Sr were separated in 2.5 N HCl using Bio-Rad AG50W-X12, 200–400 mesh cation  
107 exchange resin. Sm and Nd were separated in 0.15 N HCl using P507 cation exchange resin. The strontium (Sr) and  
108 neodymium (Nd) isotopic compositions of the sediment samples were measured using a Thermo Scientific Multi-Collector

109 Inductively Coupled Plasma Mass Spectrometer (MC-ICPMS Nu plasma) at the Key Lab of Marine Sedimentology and  
110 Environmental Geology, Ministry of Natural Resources, China. The organic materials and carbonate were removed from  
111 the samples by H<sub>2</sub>O<sub>2</sub> and HCl, respectively. For the convenience of direct comparison, the Nd isotopic ratio results are  
112 expressed as  $\epsilon\text{Nd}(0) = \left[ \frac{^{143}\text{Nd}/^{144}\text{Nd}}{0.512638} - 1 \right] \times 10000$ , using the present CHUR value (Jacobsen and Wasserburg,  
113 1980). Replicate analyses of NBS-987 during the study gave a mean  $^{87}\text{Sr}/^{86}\text{Sr}$  of  $0.710310 \pm 0.000003$  (2s), close to its  
114 certified value of 0.710245. Similarly, replicate analyses of JNDi-1 gave a mean  $^{143}\text{Nd}/^{144}\text{Nd}$  of  $0.512112 \pm 0.000004$  (2s),  
115 and its certified value was 0.511860.

### 116 3. Results

117 The age model is built based on 10 radiocarbon dates from core 17I106. The top age is 3.8 ka BP, and the bottom age is  
118 44.9 ka BP; thus, this core covers a continuous sedimentary succession of the last ~45,000 years. The sedimentation rates  
119 in the Holocene (average 3.1 cm/ka) were relatively lower than those during the last glacial period (average 4.6 cm/ka),  
120 with the highest rate of 8.3 cm/ka during 12.5–13.6 ka BP (Figure 3a). In the study core, the illite percentage ranges from  
121 31% to 63% with an average of 48%, while the smectite percentage ranges between 8% and 57% with an average of 30%  
122 (Figure 3b-e). Moreover, the kaolinite percentage ranges from 2% to 16%, and the chlorite percentage ranges from 5% to  
123 20% in the core sediments. In the study core, the  $^{87}\text{Sr}/^{86}\text{Sr}$  ratios range from 0.7122015 to 0.7186141 with an average of  
124 0.7161698, while  $\epsilon\text{Nd}$  values range from -13.02 to -10.29 with an average of -11.24 (Figure 3). At this study core, the  
125  $^{87}\text{Sr}/^{86}\text{Sr}$  ratio and  $\epsilon\text{Nd}$  values remain stable before the LGM but show fluctuations after the LGM, without obvious  
126 increasing/decreasing tendencies. During ~14.5-12.5 ka,  $^{87}\text{Sr}/^{86}\text{Sr}$  ratios significantly increased from 0.7139 to 0.7172,  
127 while  $\epsilon\text{Nd}$  values decreased abruptly from -10.28 to -13.02.

### 128 4. Discussion

#### 129 4.1. Sediment provenance and transport patterns

130 The lower sedimentation rates (3-5 cm/ka) measured in core 17I106 were in accordance with the normal sedimentation  
131 rates obtained from neighboring cores around the Ninetyeast Ridge (Ahmad et al., 2005; Raza et al., 2013). In this region,  
132 turbidite activities were less developed (Joussain et al., 2016; Fournier et al., 2017), in accordance with its far distance  
133 from the Active Channel (Figure 1). In the northern BoB, due to heavy river runoff and steep topography, the G-B river  
134 system transports a large amount of the products of Himalayan physical denudation; these products mainly consist of illite  
135 and chlorite formed under dry and cold climate conditions (Chamley, 1989; Khan et al., 2019). Because of the hot and  
136 humid conditions in Myanmar and the Indian Peninsula, sediments in these regions are formed through the chemical  
137 weathering of silicate minerals and thus have high smectite percentages. Moreover, the Irrawaddy River brought weathered  
138 products characterized by high smectite percentages from Myanmar into the Andaman Sea, leading to high smectite  
139 percentages in the terrestrial sediments deposited in this marine environment (Ali et al., 2015).

140 The relatively high illite percentages measured in core 17I106 indicate that the weathered Himalayan materials carried  
141 by the G-B River system are the primary source of sediments in the study area (Figure 4a). Compared with the large  
142 amounts of materials loaded by the G-B River system, the weathered areas and runoff volumes of the Indo-Burman Ranges  
143 are relatively small, and consequently, their sediment contributions are limited in the study area, although their sediments  
144 are also characterized by relatively high illite percentages (Joussain et al., 2016). Evidence of surface sediments in the BoB  
145 further reveals that the smectite percentages of sediments in the central region are significantly lower than those in the  
146 eastern and western regions (Li et al., 2017; Liu et al., 2019), indicating that sediments of Indian Peninsula origin are  
147 difficult to transport into the eastern BoB through the central BoB. Because the limited weathering area of Andaman and  
148 Nicobar Islands cannot provide a large amount of smectite according to provenance studies (Ali et al., 2015), the Myanmar  
149 materials characterized by high smectite percentages have the advantage of shorter transport distances compared to those  
150 sourced from the Indian Peninsula as the main source area of smectite around the BoB. Therefore, the most important  
151 source of smectite in the study area is the Myanmar region. In marine environments, kaolinite is preferentially deposited

152 in estuary areas due to mineral segregation (Gibbs, 1977) and thus may not be transported over long distances, so the  
153 kaolinite in the study area was most likely sourced from neighboring Sumatra (Figure 4a, Liu et al., 2012). The Sr-Nd  
154 isotopes measured in the studied core are close to those measured in the Irrawaddy/Indo-Burman Ranges/Sumatra source  
155 regions (Figure 4b), indicating that terrestrial materials with diameters  $<63 \mu\text{m}$  mainly come from the Irrawaddy River,  
156 Indo-Burman Ranges and Sumatra source areas, which was confirmed by a Sr-Nd isotope study in the southwestern part  
157 of the study area (Ahmad et al., 2005) and consistent with sediment provenance studies in the Ninetyeast Ridge on different  
158 timescales (Ali et al., 2021; Seo et al., 2022). This difference in clay minerals and isotopes may be consistent with the view  
159 that clay minerals may be transported over long distances, while coarser terrestrial sediments can only be transported to  
160 more proximate locations.

161 In the northeastern BoB, the southwest monsoon turns southward into the Andaman Sea, resulting in the transport of  
162 sediments from the Indo-Burman Range and Irrawaddy River to the central Andaman Sea (Colin et al., 2006). The location  
163 of core 17I106, drilled on the Ninetyeast Ridge, was above the abyssal plain, and the terrestrial materials deposited to the  
164 west of this location are difficult to resuspend and deposit on the ridge under the force of bottom currents or turbidity  
165 currents. In fact, the G-B River-loaded materials are mainly carried eastward by surface ocean currents in summer to the  
166 Andaman Sea, where the seasonal surface currents load materials from the Himalayan and Indo-Burman Ranges into the  
167 Andaman Sea through the northern strait (NS) (Liu et al., 2020a; Rayaroth et al., 2016). These G-B River sediments can  
168 also be transported southward along the west side of the Andaman and Nicobar Islands (Figure 5), and a westward ocean  
169 surface current in the middle strait (MS) loads sediments of the Irrawaddy River southwest into the study area (Chatterjee  
170 et al., 2017).

#### 171 **4.2. Factors affecting sediment provision**

172 In general, illite is the major mineral produced during the strong physical erosion of metamorphic rocks and granite rocks



173 and during the reprocessing of sedimentary rocks (Chamley, 1989; Winkler et al., 2002), while smectite is the secondary  
174 mineral produced during the chemical weathering of parent aluminosilicate and iron-magnesium silicate under warm and  
175 humid climate conditions (Chamley, 1989; Erosion, 1995). The climatic forces from the North Atlantic are thought to  
176 extensively impact the tropical Eastern Indian Ocean (EIO) and surrounding areas of the BoB (Sun et al., 2011; DiNezio  
177 and Tierney, 2013; Dutt et al., 2015; Gautam et al., 2020; Mohtadi et al., 2014; Liu et al., 2021), whose climate signals can  
178 be transmitted via the tropical Atlantic bipolar SST anomaly and associated southward shift of the ITCZ (Marzin et al.,  
179 2013), westerlies teleconnection and sea ice (Sun et al., 2011) or the reorganization of the Hadley circulation (Mohtadi et  
180 al., 2014). During the North Atlantic cold-climate periods (Heinrich events and YD period, Figure 3h), when rainfall and  
181 temperatures decreased in the South Asian monsoon region (An et al., 2011; DiNezio and Tierney, 2013; Gautam et al.,  
182 2020), physical weathering was enhanced in the Himalayas (Joussain et al., 2016), which made illite percentages at core  
183 17I106 relatively high during these cold-climate periods, but chemical weathering weakened in Myanmar, and the smectite  
184 percentage thus decreased in the source area before these cold periods and continued to increase after these periods. The  
185 increasing (decreasing) trend of illite (smectite) percentages before cold-climate periods and the decreasing (increasing)  
186 trend of illite (smectite) percentages after cold-climate periods in our records suggest that the weathering degree in the  
187 source area influenced the supply of clay minerals during these cold-climate periods.

188 Sea level fluctuation is also critical in controlling the supplementation of terrestrial materials, especially clay minerals  
189 (Li et al., 2018; Liu et al., 2019), by changing the transport paths and/or distances as well as the further input of sediments  
190 into the study area. The changing trends of the sea level in seas adjacent to the BoB (Figure 3i, Waelbroeck et al., 2002;  
191 Grant et al., 2014; Hanebuth et al., 2000; Thompson and Goldstein, 2006) are well correlated with the smectite percentages  
192 measured in core 17I106, especially during 35-21 ka, when the smectite percentages declined continuously. Since the  
193 Andaman and Nicobar Islands connecting the Andaman Sea and the BoB have continuously expanded as the sea level has  
194 continuously declined, the strait width has been consistently reduced, thereby preventing the entrance of terrestrial

195 materials into the Andaman Sea and the further continuous decline in smectite percentages in the study area. Here, we  
196 suggest that the variations in the measured illite percentages were mainly caused by changes in smectite deposition because  
197 the sedimentary records obtained from the northern BoB do not support the controlling effect of sea level on illite  
198 percentages over the past 50 ka (Joussain et al., 2016; Li et al., 2018; Liu et al., 2019). The relative exposure of 200 km  
199 from the current Irrawaddy River delta may affect the deposition process on the continental shelf or further deposition of  
200 the sediments delivered to the deep ocean, but core 17I106 is formed by the long-distance transport of large amounts of  
201 fine-grained terrestrial material, indicating that these sediments can be transported over long distances, and the ~200 km  
202 change in the shelf distance is not a dominant factor of sediment transport in the study area. Moreover, the decreasing  
203 smectite percentages from the Myanmar area as sea level decreases suggests that shelf denudation is also not the main  
204 factor affecting our smectite record, which is in accordance with previous studies in the Andaman Sea that have not  
205 specifically emphasized the alteration of terrestrial source material supply by exposed shelves (Ali et al., 2015; Awasthi et  
206 al., 2014).

207 The South Asian summer monsoon is normally thought to be an important factor affecting weathering conditions  
208 around the BoB (Dutt et al., 2015; Gebregiorgis et al., 2016; Joussain et al., 2017; Li et al., 2018; Rashid et al., 2011; Zhang  
209 et al., 2020; Zorzi et al., 2015). Stalagmites in Mawmluh Cave record variations in river runoff in the surrounding area;  
210 these variations are determined by the impacts of SST and water vapor transport paths (Dutt et al., 2015). In fact, the  
211 Mawmluh Cave records of the South Asian monsoon strength are driven by temperature gradients that drive changes in  
212 winds and moisture transport into the BoB (Dutt et al., 2015), not just responding to the rainfall amount. The smectite  
213 percentage changes measured in core 17I106 were slightly correlated after Heinrich event 1 (H1) but were irrelevant before  
214 H1 (Figure 6b). This indicated that the combination of temperature and moisture failed to play a crucial role in smectite  
215 transport to core 17I106, although weathering features in the source area may be shaped by the South Asian monsoon.  
216 Moreover, the view could be confirmed by the smectite record obtained from the studied core not being well correlated

217 with records previously obtained in the Andaman Sea (Figure 6c, 6d, Gebregiorgis et al., 2016) or with a sporopollen record  
218 obtained in Southwest China (Figure 6e, 6f, Zhang et al., 2020), especially before the LGM. The consistency of salinity  
219 and SST in core SK 168 (Figure 6c, 6d) and moisture and temperature index (Figure 6e, 6f) in Southwest China reveal that  
220 the hydroclimate in the South Asian monsoon region might have been influenced by SST in the Indian Ocean. All these  
221 inconsistencies between the smectite percentage in core 17I106 and monsoon records indicate that smectite  
222 supplementation may be mainly controlled by rainfall rather than by chemical weathering due to thermodynamic  
223 differences between sea and land environments (Liu et al., 2020b).

224 During the late LGM, the smectite percentage increased abnormally in core 17I106, and this increase cannot be  
225 explained by dry and cold weathering conditions, a lower sea level or a weakened summer monsoon at that time. In contrast,  
226 this abnormal change may have been attributed to an increase in the smectite input in sediments from the Burman source  
227 area or to a decrease in the amounts of sediment input from the Himalayas. Under the influence of the winter monsoon  
228 during the LGM, the denuded sediments on the Irrawaddy Estuary shelf may have been transported southward through the  
229 west side of Andaman Island (Prajith et al., 2018), as was confirmed in previous work showing that the winter monsoon  
230 led to an increase in terrestrial materials from the Irrawaddy River to the Ninetyeast Ridge during the Heinrich event  
231 (Ahmad et al., 2005). However, the winter monsoon was strong in the western part of the study area from 21 to 15 ka  
232 (Figure 6g), and the sea level remained relatively low during that period (Gautam et al., 2020). The smectite percentages  
233 in the studied core increased significantly from 21 to 19 ka and dropped rapidly after 19 ka. This inconsistency contradicts  
234 the conclusion that the increased smectite percentage in the source area was caused by a strong winter monsoon. Moreover,  
235 the changes in the sediment compositions measured in the Himalayan source area were probably related to variations in  
236 regional glaciers. During the LGM period, the increased glacial cover may have reduced surface runoff and furthered the  
237 transport of physical weathering products, while the increased amount of ice meltwater may have transported more illites  
238 following glacial melt. However, the reduced glacial area in the Himalayas during 18-15 ka did not occur simultaneously

239 with the increased illite percentage (Yan et al., 2020; Weldeab et al., 2019, Figure 6h). Therefore, the abnormal changes  
240 measured in the smectite percentage during the late LGM period were caused by other climate-driven mechanisms, and the  
241 millennium-scale smectite percentage fluctuations that occurred before the LGM require a more reasonable explanation.

#### 242 **4.3. The ITCZ shift in the EIO**

243 Changes in rainfall and the corresponding runoff are generally utilized to explain short-term variations in clay minerals. In  
244 the EIO, rainfall is controlled by monsoon activities (An et al., 2011; Beck et al., 2018; Gebregiorgis et al., 2016) and/or  
245 ITCZ migrations (Deplazes et al., 2013; Stoll et al., 2007; Tan et al., 2019). Glacial-interglacial monsoon precipitation  
246 changes at the regional scale are shaped by dynamics (changes in the wind fields) and temperature (McGee, 2020). The  
247 wind fields may be driven by the relative dominance of the northern low-pressure and southern high-pressure systems (An  
248 et al., 2011) and cross-equatorial moisture transport (Clemens et al., 2021), while the SST in the eastern Indian Ocean  
249 (Zhang et al., 2020) or western Indian Ocean (Wang et al., 2022), surface and subsurface temperature changes (Tierney et  
250 al., 2015), and temperature gradients (Weldeab et al., 2022) also play an important role in South Asian rainfall. At the same  
251 time, as a climate-driving force in low-latitude regions, ITCZ migrations may be the main factor responsible for regional  
252 hydrological changes (Deplazes et al., 2013; Weber et al., 2018) since the shift in the ITCZ was considered to control  
253 rainfall distribution and intensity in central India over geological time scales (Zorzi et al., 2015) and to cause summer  
254 temperature and moisture fluctuations in southwestern China during the last deglaciation (Zhang et al., 2019).

255 During the glacial-interglacial period, the ITCZ migrated north-south and balanced thermal differences by transferring  
256 atmospheric heat; this process represents an indispensable climate-regulating power on Earth (Broccoli et al., 2006; McGee  
257 et al., 2018; Schneider et al., 2014). In the Cariaco Basin and Arabian Seas (Figure 7), tropical rainfall is highly correlated  
258 with the North Atlantic climate, and sea ice variations in the North Atlantic affect the north-south shift of the ITCZ in low-  
259 latitude regions through atmospheric circulation and ocean processes (Deplazes et al., 2013). The smectite particles

260 measured in core 17I106 mainly came from the Myanmar source area; in this area, rainfall is greatly affected by the seasonal  
261 shift of the ITCZ. Before the LGM, the smectite percentages in the study core were well matched with the ITCZ record in  
262 the Arabian Sea, where the supplementation of smectite percentages reached the peak when the ITCZ shifted significantly  
263 northward (Deplazes et al., 2013). During cold climate events, when the ITCZ moved significantly southward, rainfall  
264 decreased, and the smectite percentages decreased correspondingly in the source area. Therefore, we suggest that these  
265 changes in the smectite percentages in the studied core are correlated with ITCZ migration and that rainfall is an important  
266 factor determining the smectite percentage from the source area of Myanmar on the millennial scale. The sporopollen  
267 evidence suggested a cold and wet period during MIS 3 in Yunnan, China (Zhang et al., 2020), which may have been  
268 caused by the frequent northward movement of the ITCZ during this period. If precipitation induced by wind and  
269 temperature of the South Asian monsoon have an intense impact on the source area, the source area monsoon indicators,  
270 for example, foraminifera, sporopollen, stalagmite (Figure 6) and other indicators, would correspondingly change, but our  
271 record failed to catch these variations in monsoon indicators in the BoB. We suggest that every factor affecting precipitation  
272 induced by wind and temperature of the South Asian monsoon, as mentioned above, may have made it difficult to cause  
273 millennial-scale fluctuations similar to the ITCZ shift during the MIS3 period. The South Asian monsoon is indeed the  
274 result of combined factors that may contribute to the heterogeneity of monsoon rainfall in the BoB, which were also  
275 influenced by the north-south shift of the ITCZ. In core 17I106, the corresponding variations in the relatively high smectite  
276 percentages and the northward shift of the ITCZ indicate that the northward movement of the ITCZ is the most important  
277 factor influencing the incremental changes in river sediment load corresponding to the increased smectite percentages in  
278 the Myanmar region. Here we emphasize that the northward and southward ITCZ shifts bring about rainfall increases and  
279 decreases relative to other rainfall forces. The changes in clay minerals reflect changes in clay mineral supply in the source  
280 area, and it is that these relative increases and decreases in rainfall lead to changes, which is a response to environmental  
281 changes. The sporopollen evidence suggested a cold and wet period during MIS3 in Yunnan, China (Zhang et al., 2020),

282 which may have been caused by the frequent northward movement of the ITCZ during this period.

283 Although the changes in smectite percentages in the study area are associated with ITCZ shifts before the LGM, the  
284 ITCZ shift in the Indo-Pacific warm pool (IPWP) was more “regional” than those in the Arabian Sea and the Cariaco Basin  
285 (Deplazes et al., 2013). During the late LGM, when the ITCZ did not move extensively in the Arabian Sea, the ITCZ  
286 gradually shifted northward in the IPWP from 21-18 ka (Figure 7, Ayliffe et al., 2013). However, the smectite percentage  
287 increased significantly in the study area, and we have excluded the possibility that the winter monsoon or meltwater  
288 influenced these changes. Further comparisons with IPWP records reveal that the ITCZ changes agree well with the  
289 smectite percentage variations during the late LGM, indicating that the northern migration of the ITCZ induced high  
290 smectite percentages in core 17I106 (Figure 7c, d). These results suggest that the clay minerals of core 17I106 are  
291 inextricably linked to ITCZ shifts on the millennial scale. In summary, our smectite record shows that before the LGM, the  
292 ITCZ was in a relatively southerly position in the Myanmar area, while during the late LGM, the northward movement of  
293 the ITCZ in the BoB led to increased rainfall in the Myanmar source area and an increased supply of smectite. At the same  
294 time, the ITCZ was not significantly shifted in the Arabian Sea region either pre-LGM or post-LGM, which is what the  
295 Arabian Sea record shows (Deplaze et al., 2013).

296 The smectite percentage in the studied core is different from the ITCZ records in some periods, such as the late LGM,  
297 revealing that regional changes in the ITCZ were significantly obvious and that the ITCZ is not a simple N-S displacement.  
298 This consistency may indicate that the regional extension of the north-south thermodynamic gradient in the EIO exceeded  
299 that in the Arabian Sea and that the north-south shift of the ITCZ caused the climate systems of the Northern and Southern  
300 Hemispheres to be more closely connected in the EIO during the late LGM (Huang et al., 2019; Zhuravleva et al., 2021).  
301 A recent study considered less northward migration of the summer ITCZ position in the western BoB than in the eastern  
302 BoB during Heinrich Stadials HS1 and HS5 (Ota et al., 2022), which indicated that regional ITCZ variations in the BoB  
303 may be very common. These factors may be correlated with observed variations in regional air-sea interactions, such as

304 the exposure of the Sunda Shelf (DiNezio and Tierney, 2013), the effect of the thermocline in the EIO (Mohtadi et al., 2017)  
305 and even potential El Nino-like mode (Thirumalai et al., 2019) and IOD (Abram et al., 2020) changes, which may make  
306 the ITCZ shift more dramatic or keep the ITCZ position in the Northern Hemisphere longer. Thus, the regional variations  
307 in the ITCZ should be fully considered when studying climate change, especially in low-latitude regions that are sensitive  
308 to climatic and environmental changes, such as the EIO (Niedermeyer et al., 2014).

## 309 **5. Conclusion**

310 We reconstructed the variations in sediment sources on the Ninetyeast Ridge over the past 45 ka. The main source areas  
311 comprise the Himalayas transported by the G-B River and Irrawaddy River; sediments were stably supplied from these  
312 regions throughout the studied core. When North Atlantic cold events (Heinrich and YD) occurred, chemical weathering  
313 weakened and physical weathering increased; correspondingly, the smectite percentage decreased and the illite percentage  
314 increased. From 35-21 ka, the falling sea level led to an increase in the exposed area of the Andaman and Nicobar Islands  
315 and further hindered the entrance of smectite from the Andaman Sea into the study area. At the same time, the influence of  
316 the South Asian monsoon on the sediment supply was not obvious. The time-phase mismatches observed among records  
317 excluded the influence of Burman shelf sediment erosion forced by the winter monsoon or of variations in G-B river  
318 sediments induced by ice meltwater on the abnormal increases observed in the smectite percentages during the late LGM.  
319 The smectite record of core 17I106 is consistent with the ITCZ changes recorded on the millennial scale, indicating that  
320 the ITCZ controls the rainfall in the Burman source area and, further, the clay mineral variations in the study area. The  
321 inferred ITCZ shift recorded in the studied core coincided with the global ITCZ change that occurred before the LGM, but  
322 during the late LGM, the core record was consistent with the change in the regional ITCZ recorded by the IPWP. This  
323 revealed that regional changes in the ITCZ were very significant, and the ITCZ is not a simple N-S displacement at the  
324 same time. Thus, the regional variations in the ITCZ should be fully considered when studying climate change, especially  
325 in low-latitude regions that are sensitive to climate and environmental changes.

326 **Author contributions.**

327 J.L. and Y.H. conceived and designed the experiment. X.X. wrote the manuscript with contributions from all authors. L.Z.  
328 and L.Y. provided the ages of planktonic foraminifera, and S.L., Y.Y., L.C., and L.T. helped to analyze the measured data  
329 and discuss the related relevant topics in this manuscript.

330 **Competing interests.**

331 The authors declare that they have no conflicts of interest.

332 **Acknowledgements.**

333 We thank Hui Zhang for the Sr-Nd isotope measurements. Core sediment samples were collected onboard of R/V “Shiyan  
334 1” implementing the open research cruise NORC 2012-08 supported by the NSFC Shiptime Sharing Project.

335 **Financial support.**

336 This work has been jointly funded by the National Natural Science Foundation of China (42176075, 42130412 and  
337 41576044), Key Special Project for Introduced Talents Team of Southern Marine Science and Engineering Guangdong  
338 Laboratory (Guangzhou) (GML2019ZD0206), and the Open Fund of the Key Laboratory of Submarine Geosciences,  
339 Ministry of Natural Resources (KLSG2102).

340 **Data Availability Statement.**

341 All dataset is available on Science Data Bank  
342 (<https://www.scidb.cn/detail?dataSetId=55c7dcf1f8344c658099dfe030264b2f>).

343 **References**

344 Abram, N.J., Hargreaves, J.A., Wright, N.M., Thirumalai, K., Ummenhofer, C.C., and England, M.H.: Palaeoclimate



345 perspectives on the Indian Ocean Dipole, *Quat. Sci. Rev.*, 237, 106302,  
346 <https://doi.org/10.1016/j.quascirev.2020.106302>, 2020.

347 Ahmad, S.M., Anil Babu, G., Padmakumari, V.M., Dayal, A.M., Sukhija, B.S., and Nagabhushanam, P.: Sr, Nd isotopic  
348 evidence of terrigenous flux variations in the Bay of Bengal: Implications of monsoons during the last ~34,000 years,  
349 *Geophys. Res. Lett.*, 32, L22711, <https://doi.org/10.1029/2005GL024519>, 2005.

350 Ahmad, S.M., Padmakumari, V.M. and Babu, G.A.: Strontium and neodymium isotopic compositions in sediments from  
351 Godavari, Krishna and Pennar rivers, *Curr. Sci.*, 97, 1766-1769, 2009.

352 Ali, S., Hathorne, E.C., Frank, M., Gebregiorgis, D., Stattegger, K., Stumpf, R., Kutterolf, S., Johnson, J.E., and Giosan,  
353 L.: South Asian monsoon history over the past 60 kyr recorded by radiogenic isotopes and clay mineral assemblages  
354 in the Andaman Sea, *Geochem., Geophys., Geosy.*, 16, 505-521, <https://doi.org/10.1002/2014gc005586>, 2015.

355 Ali, S., Hathorne, E.C., and Frank, M.: Persistent Provenance of South Asian Monsoon-Induced Silicate Weathering Over  
356 the Past 27 Million Years, *Paleoceanogr. Paleocl.*, 36, e2020PA003909, <https://doi.org/10.1029/2020PA003909>, 2021.

357 An, Z., Clemens, S., Shen, J., Qiang, X., Jin, Z., Sun, Y., Prell, W., Luo, J., Wang, S., Xu, H., Cai, Y., Zhou, W., Liu, X.,  
358 Liu, W., Shi, Z., Yan, L., Xiao, X., Chang, H., Wu, F., Ai, L., and Lu, F.: Glacial-Interglacial Indian Summer Monsoon  
359 Dynamics, *Science*, 333, 719-723, <https://doi.org/10.1126/science.1203752>, 2011.

360 Awasthi, N., Ray, J.S., Singh, A.K., Band, S.T., and Rai, V.K.: Provenance of the Late Quaternary sediments in the Andaman  
361 Sea: Implications for monsoon variability and ocean circulation, *Geochem., Geophys., Geosy.*, 15, 3890-3906,  
362 <https://doi.org/10.1002/2014gc005462>, 2014.

363 Ayliffe, L.K., Gagan, M.K., Zhao, J.X., Drysdale, R.N., Hellstrom, J.C., Hantoro, W.S., Griffiths, M.L., Scott-Gagan, H.,  
364 Pierre, E.S., Cowley, J.A., and Suwargadi, B.W.: Rapid interhemispheric climate links via the Australasian monsoon  
365 during the last deglaciation, *Nat. Commun.*, 4, 2908, <https://doi.org/10.1038/ncomms3908>, 2013.

366 Beck, J.W., Zhou, W., Li, C., Wu, Z., White, L., Xian, F., Kong, X.H., and An, Z.: A 550,000-year record of East Asian

367 monsoon rainfall from Be-10 in loess, *Science*, 360, 877-881, <https://doi.org/10.1126/science.aam5825>, 2018.

368 Bejugam, P., and Nayak, G.N.: Source and depositional processes of the surface sediments and their implications on  
369 productivity in recent past off Mahanadi to Pennar River mouths, western Bay of Bengal, *Palaeogeogr.,*  
370 *Palaeoclimatol., Palaeoecol.*, 483, 58-69, <https://doi.org/10.1016/j.palaeo.2016.12.006>, 2017.

371 Biscaye, P.E.: Mineralogy and sedimentation of recent deep-sea clay in Atlantic Ocean and adjacent seas and oceans, *Geol.*  
372 *Soc. Amer. Bull.*, 76, 803-832, [https://doi.org/10.1130/0016-7606\(1965\)76\[803:masord\]2.0.co;2](https://doi.org/10.1130/0016-7606(1965)76[803:masord]2.0.co;2), 1965.

373 Blaauw, M., and Christen, J.A.: Flexible Paleoclimate Age-Depth Models Using an Autoregressive Gamma Process,  
374 *Bayesian Analysis*, 6, 457-474, <https://doi.org/10.1214/11-ba618>, 2011.

375 Broccoli, A.J., Dahl, K.A., and Stouffer, R.J.: Response of the ITCZ to Northern Hemisphere cooling, *Geophys. Res. Lett.*,  
376 33, L01702, <https://doi.org/10.1029/2005GL024546>, 2006.

377 Chamley, H.: *Clay Sedimentology*, Springer, Berlin, 623 pp., 1989.

378 Chatterjee, A., Shankar, D., McCreary, J.P., Vinayachandran, P.N., and Mukherjee, A.: Dynamics of Andaman Sea  
379 circulation and its role in connecting the equatorial Indian Ocean to the Bay of Bengal, *J. Geophys. Res. Oceans*, 122,  
380 3200-3218, <https://doi.org/10.1002/2016JC012300>, 2017.

381 Clemens, S.C., Yamamoto, M., Thirumalai, K., Giosan, L., Richey, J.N., Nilsson-Kerr, K., Rosenthal, Y., Anand, P.,  
382 McGrath, S.M.: Remote and local drivers of Pleistocene South Asian summer monsoon precipitation: A test for future  
383 predictions. *Sci. Adv.*, 7(23), eabg3848. <https://doi.org/10.1126/sciadv.abg3848>, 2021.

384 Colin, C., Turpin, L., Bertaux, J., Desprairies, A., and Kissel, C.: Erosional history of the Himalayan and Burman Ranges  
385 during the last two glacial-interglacial cycles, *Earth Planet. Sci. Lett.*, 171, 647-660, <https://doi.org/10.1016/s0012->  
386 [821x\(99\)00184-3](https://doi.org/10.1016/s0012-821x(99)00184-3), 1999.

387 Colin, C., Turpin, L., Blamart, D., Frank, N., Kissel, C., and Duchamp, S.: Evolution of weathering patterns in the Indo-  
388 Burman Ranges over the last 280 kyr: Effects of sediment provenance on  $^{87}\text{Sr}/^{86}\text{Sr}$  ratios tracer, *Geochem., Geophys.*,

389 Geosy., 7, Q03007, <https://doi.org/10.1029/2005gc000962>, 2006.

390 Curray, J.R., Emmel, F.J., and Moore, D.G.: The Bengal Fan: morphology, geometry, stratigraphy, history and processes,  
391 Mar. Petrol. Geol., 19, 1191-1223, [https://doi.org/10.1016/S0264-8172\(03\)00035-7](https://doi.org/10.1016/S0264-8172(03)00035-7), 2003.

392 Deplazes, G., Lückge, A., Peterson, L.C., Timmermann, A., Hamann, Y., Hughen, K.A., Röhl, U., Laj, C., Cane, M.A.,  
393 Sigman, D.M., and Haug, G.H.: Links between tropical rainfall and North Atlantic climate during the last glacial  
394 period, Nat. Geosci., 6, 213-217, <https://doi.org/10.1038/ngeo1712>, 2013.

395 DiNezio, P.N., and Tierney, J.E.: The effect of sea level on glacial Indo-Pacific climate, Nat. Geosci., 6, 485-491,  
396 <https://doi.org/10.1038/ngeo1823>, 2013.

397 Dou, Y., Yang, S., Shi, X., Clift, P.D., Liu, S., Liu, J., Li, C., Bi, L., and Zhao, Y.: Provenance weathering and erosion  
398 records in southern Okinawa Trough sediments since 28 ka: Geochemical and Sr–Nd–Pb isotopic evidences, Chem.  
399 Geol., 425, 93-109. <https://doi.org/10.1016/j.chemgeo.2016.01.029>, 2016.

400 Dutt, S., Gupta, A.K., Clemens, S.C., Cheng, H., Singh, R.K., Kathayat, G., and Edwards, R.L.: Abrupt changes in Indian  
401 summer monsoon strength during 33,800 to 5500 years B.P., Geophys. Res. Lett., 42, 5526-5532,  
402 <https://doi.org/10.1002/2015gl064015>, 2015.

403 Erosion, H.S.: Sedimentation and sedimentary origin of clays, in: Velde, B. (Ed.), Origin and Mineralogy of Clays. Clays  
404 Environment., Springer, Berlin, pp. 162-219, 1995.

405 Fournier, L., Fauquembergue, K., Zaragosi, S., Zorzi, C., Malaize, B., Bassinot, F., Joussain, R., Colin, C., Moreno, E., and  
406 Leparmentier, F.: The Bengal fan: external controls on the Holocene Active Channel turbidite activity, Holocene, 27  
407 (6), 900-913, <https://doi.org/10.1177/0959683616675938>, 2017.

408 Gautam, P.K., Narayana, A.C., Kumar, P.K., Bhavani, P.G., Yadava, M.G., and Jull, A.J.T.: Indian monsoon variability  
409 during the last 46 kyr: isotopic records of planktic foraminifera from southwestern Bay of Bengal, J. Quat. Sci., 36,  
410 138-151, <https://doi.org/10.1002/jqs.3263>, 2020.

411 Gebregiorgis, D., Hathorne, E.C., Sijinkumar, A.V., Nath, B.N., Nürnberg, D., and Frank, M.: South Asian summer  
412 monsoon variability during the last ~54 kyrs inferred from surface water salinity and river runoff proxies, *Quat. Sci.*  
413 *Rev.*, 138, 6-15, <https://doi.org/10.1016/j.quascirev.2016.02.012>, 2016.

414 Gibbs, R.J.: Clay mineral segregation in the marine environment, *J. Sediment. Res.*, 47, 237-243, 1977.

415 Goodbred, S.L., and Kuehl, S.A.: Enormous Ganges-Brahmaputra sediment discharge during strengthened early Holocene  
416 monsoon, *Geology*, 28, 1083-1086, [https://doi.org/10.1130/0091-7613\(2000\)028<1083:Egbsdd>2.3.Co;2](https://doi.org/10.1130/0091-7613(2000)028<1083:Egbsdd>2.3.Co;2), 2000.

417 Grant, K.M., Rohling, E.J., Ramsey, C.B., Cheng, H., Edwards, R.L., Florindo, F., Heslop, D., Marra, F., Roberts, A.P.,  
418 Tamisiea, M.E., and Williams, F.: Sea-level variability over five glacial cycles, *Nat. Commun.*, 5, 5076,  
419 <https://doi.org/10.1038/ncomms6076>, 2014.

420 Hanebuth, T., Stattegger, K., and Grootes, P.M.: Rapid Flooding of the Sunda Shelf: A Late-Glacial Sea-Level Record,  
421 *Science*, 288, 1033-1035, <https://doi.org/10.1126/science.288.5468.1033>, 2000.

422 Huang, J., Wan, S., Li, A., and Li, T.: Two-phase structure of tropical hydroclimate during Heinrich Stadial 1 and its global  
423 implications, *Quat. Sci. Rev.*, 222, 105900, <https://doi.org/10.1016/j.quascirev.2019.105900>, 2019.

424 Jacobsen, S.B. and Wasserburg, G.J.: Sm-Nd isotopic evolution of chondrites, *Earth Planet. Sci. Lett.*, 50, 139-155,  
425 [https://doi.org/10.1016/0012-821x\(80\)90125-9](https://doi.org/10.1016/0012-821x(80)90125-9), 1980.

426 Jousain, R., Colin, C., Liu, Z., Meynadier, L., Fournier, L., Fauquembergue, K., Zaragosi, S., Schmidt, F., Rojas, V., and  
427 Bassinot, F.: Climatic control of sediment transport from the Himalayas to the proximal NE Bengal Fan during the  
428 last glacial-interglacial cycle, *Quat. Sci. Rev.*, 148, 1-16, <https://doi.org/10.1016/j.quascirev.2016.06.016>, 2016.

429 Jousain, R., Liu, Z., Colin, C., Duchamp-Alphonse, S., Yu, Z., Moréno, E., Fournier, L., Zaragosi, S., Dapigny, A.,  
430 Meynadier, L., and Bassinot, F.: Link between Indian monsoon rainfall and physical erosion in the Himalayan system  
431 during the Holocene, *Geochem., Geophys., Geosy.*, 18, 3452-3469, <https://doi.org/10.1002/2016gc006762>, 2017.

432 Kessarkar, P.M., Rao, V.P., Ahmad, S.M., Patil, S.K., Kumar, A.A., Babu, G.A., Chakraborty, S., and Rajan, R.S.: Changing

433 sedimentary environment during the Late Quaternary: Sedimentological and isotopic evidence from the distal Bengal  
434 Fan, *Deep Sea Res. Pt I: Oceanogr. Res. Papers*, 52, 1591-1615, <https://doi.org/10.1016/j.dsr.2005.01.009>, 2005.

435 Khan, M.H.R., Liu, J., Liu, S., Seddique, A.A., Cao, L., and Rahman, A.: Clay mineral compositions in surface sediments  
436 of the Ganges-Brahmaputra-Meghna river system of Bengal Basin, Bangladesh, *Mar. Geol.*, 412, 27-36,  
437 <https://doi.org/10.1016/j.margeo.2019.03.007>, 2019.

438 Li, J., Liu, S., Shi, X., Feng, X., Fang, X., Cao, P., Sun, X.Q., Ye, W.X., Khokiattiwong, S., and Kornkanitnan, N.:  
439 Distributions of clay minerals in surface sediments of the middle Bay of Bengal: Source and transport pattern,  
440 *Continent. Shelf Res.*, 145, 59-67, <https://doi.org/10.1016/j.csr.2017.06.017>, 2017.

441 Li, J., Liu, S., Shi, X., Zhang, H., Fang, X., Chen, M.-T., Cao, P., Sun, X. Q., Ye, W.X., Wu, K.K., Khokiattiwong, S., and  
442 Kornkanitnan, N.: Clay minerals and Sr-Nd isotopic composition of the Bay of Bengal sediments: Implications for  
443 sediment provenance and climate control since 40 ka, *Quat. Internat.*, 493, 50-58,  
444 <https://doi.org/10.1016/j.quaint.2018.06.044>, 2018.

445 Licht, A. France-Lanord, C., Reisberg, L., Fontaine, C., Soe, A.N., and Jaeger, J.J.: A palaeo Tibet-Myanmar connection?  
446 Reconstructing the Late Eocene drainage system of central Myanmar using a multi-proxy approach, *J. Geol. Soc.*,  
447 170, 929-939, <https://doi.org/10.1144/jgs2012-126>, 2013.

448 Liu, J., He, W., Cao, L., Zhu, Z., Xiang, R., Li, T., Shi, X., and Liu, S.: Staged fine-grained sediment supply from the  
449 Himalayas to the Bengal Fan in response to climate change over the past 50,000 years, *Quat. Sci. Rev.*, 212, 164-177,  
450 <https://doi.org/10.1016/j.quascirev.2019.04.008>, 2019.

451 Liu, J P., Kuehl, S.A., Pierce, A.C., Williams, J., Blair, N.E., Harris, C., Aung, D.W., and Aye, Y.Y.: Fate of Ayeyarwady  
452 and Thanlwin Rivers Sediments in the Andaman Sea and Bay of Bengal, *Mar. Geol.*, 423, 106137,  
453 <https://doi.org/10.1016/j.margeo.2020.106137>, 2020a.

454 Liu, S., Li, J., Zhang, H., Cao, P., Mi, B., Khokiattiwong, S., Kornkanitnan, N., and Shi, X.: Complex response of

455 weathering intensity registered in the Andaman Sea sediments to the Indian Summer Monsoon over the last 40 kyr,  
456 Mar. Geol., 426, 106206, <https://doi.org/10.1016/j.margeo.2020.106206>, 2020b.

457 Liu, S., Ye, W., Cao, P., Zhang, H., Chen, M. -T., Li, X., Li, J., Pan, H.-J., Khokiattiwong, S., Kornkanitnan, N., and Shi,  
458 X.: Paleoclimatic responses in the tropical Indian Ocean to regional monsoon and global climate change over the last  
459 42 kyr, Mar. Geol., 438, 106542, <https://doi.org/10.1016/j.margeo.2021.106542>, 2021.

460 Liu, Z., Wang, H., Hantoro, W. S., Sathiamurthy, E., Colin, C., Zhao, Y., Li, J.: Climatic and tectonic controls on chemical  
461 weathering in tropical Southeast Asia (Malay Peninsula, Borneo, and Sumatra), Chem. Geol., 291, 1-12,  
462 <https://doi.org/10.1016/j.chemgeo.2011.11.015>, 2012.

463 Lupker, M., France-Lanord, C., Galy, V., Lavé, J., and Kudrass, H.: Increasing chemical weathering in the Himalayan  
464 system since the Last Glacial Maximum, Earth Planet. Sci. Lett., 365, 243-252,  
465 <https://doi.org/10.1016/j.epsl.2013.01.038>, 2013.

466 Marzin, C., Kallel, N., Kageyama, M., Duplessy, J.C., and Braconnot, P.: Glacial fluctuations of the Indian monsoon and  
467 their relationship with North Atlantic climate: new data and modelling experiments, Clim. Past., 9, 2135-2151,  
468 <https://doi.org/10.5194/cp-9-2135-2013>, 2013.

469 McGee, D., Moreno-Chamarro, E., Green, B., Marshall, J., Galbraith, E., and Bradtmiller, L.: Hemispherically asymmetric  
470 trade wind changes as signatures of past ITCZ shifts, Quat. Sci. Rev., 180, 214-228,  
471 <https://doi.org/10.1016/j.quascirev.2017.11.020>, 2018.

472 McGee, D.: Glacial-Interglacial Precipitation Changes. Ann. Rev. Mar. Sci., 12, 525-557.  
473 <https://doi.org/10.1146/annurev-marine-010419-010859>, 2020.

474 Mohtadi, M., Prange, M., Oppo, D. W., De Pol-Holz, R., Merkel, U., Zhang, X., Steinke, S., and Luckge, A.: North Atlantic  
475 forcing of tropical Indian Ocean climate, Nature, 509, 76-80, <https://doi.org/10.1038/nature13196>, 2014.

476 Mohtadi, M., Prange, M., Steinke, S.: Palaeoclimatic insights into forcing and response of monsoon rainfall, Nature, 533,

477 191-199, <https://doi.org/10.1038/nature17450>, 2016.

478 Mohtadi, M., Prange, M., Schefuss, E., and Jennerjahn, T.C.: Late Holocene slowdown of the Indian Ocean Walker  
479 circulation, *Nat. Commun.*, 8, 1015, <https://doi.org/10.1038/s41467-017-00855-3>, 2017.

480 Niedermeyer, E.M., Sessions, A.L., Feakins, S.J., and Mohtadi, M.: Hydroclimate of the western Indo-Pacific Warm Pool  
481 during the past 24,000 years, *P. Natl. Acad. Sci. USA*, 111, 9402-9406, <https://doi.org/10.1073/pnas.1323585111>, 2014.

482 Ota, Y., Kawahata, H., Kuroda, J., Suzuki, A., Abe-Ouchi, A., and Jimenez-Espejo, F.J.: Millennial-scale variability of  
483 Indian summer monsoon constrained by the western Bay of Bengal sediments: Implication from geochemical proxies  
484 of sea surface salinity and river runoff, *Glob. Planet. Change*, 208, <https://doi.org/10.1016/j.gloplacha.2021.103719>,  
485 2022.

486 Peng, J., Yang, X., Toney, J.L., Ruan, J., Li, G., Zhou, Q., Gao, H., Xie, Y., Chen, Q., and Zhang, T.: Indian Summer  
487 Monsoon variations and competing influences between hemispheres since ~35 ka recorded in Tengchongqinghai Lake,  
488 southwestern China, *Palaeogeogr., Palaeoclimatol., Palaeoecol.*, 516, 113-125,  
489 <https://doi.org/10.1016/j.palaeo.2018.11.040>, 2019.

490 Prajith, A., Tyagi, A., and John Kurian, P.: Changing sediment sources in the Bay of Bengal: Evidence of summer monsoon  
491 intensification and ice-melt over Himalaya during the Late Quaternary, *Palaeogeogr., Palaeoclimatol., Palaeoecol.*,  
492 511, 309-318, <https://doi.org/10.1016/j.palaeo.2018.08.016>, 2018.

493 Rashid, H., England, E., Thompson, L., and Polyak, L.: Late Glacial to Holocene Indian Summer Monsoon Variability  
494 Based upon Sediment Records Taken from the Bay of Bengal, *Terr., Atmosp. Ocean. Sci.*, 22, 215-228,  
495 [https://doi.org/10.3319/TAO.2010.09.17.02\(TibXS\)](https://doi.org/10.3319/TAO.2010.09.17.02(TibXS)), 2011.

496 Rayaroth, M.K., Peter, B.N., and Mahmud, M.R.: High-resolution surface circulation of the Bay of Bengal derived from  
497 satellite observation data, *J. Mar. Sci. Technol.*, 24, 656-668, <https://doi.org/10.6119/JMST-015-1215-2>, 2016.

498 Raza, T., and Ahmad, S.M.: Surface and deep water variations in the northeast Indian Ocean during 34-6 ka BP: evidence

499 from carbon and oxygen isotopes of fossil foraminifera, *Quat. Internat.*, 298, 37-44,  
500 <https://doi.org/10.1016/j.quaint.2012.05.005>, 2013.

501 Reimer, P.J., Austin, W.E.N., Bard, E., Bayliss, A., Blackwell, P.G., Bronk Ramsey, C., Butzin, M., Cheng, H., Edwards,  
502 R.L., Friedrich, M., Grootes, P.M., Guilderson, T.P., Hajdas, I., Heaton, T.J., Hogg, A.G., Hughen, K.A., Kromer, B.,  
503 Manning, S.W., Muscheler, R., Palmer, J.G., Pearson, C., van der Plicht, J., Reimer, R.W., Richards, D.A., Scott, E.M.,  
504 Southon, J.R., Turney, C.S.M., Wacker, L., Adolphi, F., Büntgen, U., Capano, M., Fahrni, S.M., Fogtmann-Schulz, A.,  
505 Friedrich, R., Köhler, P., Kudsk, S., Miyake, F., Olsen, J., Reinig, F., Sakamoto, M., Sookdeo, A., and Talamo, S.: The  
506 intcal20 northern hemisphere radiocarbon age calibration curve (0-55 cal kBP), *Radiocarbon*, 62, 725-757,  
507 <https://doi.org/10.1017/RDC.2020.41>, 2020.

508 Rodolfo, K.S.: Sediments of Andaman Basin, northeastern Indian Ocean, *Mar. Geol.*, 7, 371-380,  
509 [https://doi.org/10.1016/0025-3227\(69\)90014-0](https://doi.org/10.1016/0025-3227(69)90014-0), 1969.

510 Schneider, T., Bischoff, T., and Haug, G.H.: Migrations and dynamics of the intertropical convergence zone, *Nature*, 513,  
511 45-53, <https://doi.org/10.1038/nature13636>, 2014.

512 Schott, F.A., and McCreary, J.P.: The monsoon circulation of the Indian Ocean, *Progr. Oceanogr.*, 51, 1-123,  
513 [https://doi.org/10.1016/s0079-6611\(01\)00083-0](https://doi.org/10.1016/s0079-6611(01)00083-0), 2001.

514 Seo, I., Khim, B.-K., Cho, H.G., Huh, Y., Lee, J., and Hyeong, K.: Origin of the Holocene Sediments in the Ninetyeast  
515 Ridge of the Equatorial Indian Ocean, *Ocean Sci. J.*, <https://doi.org/10.1007/s12601-021-00052-w>, 2022.

516 Shankar, D., Vinayachandran, P.N., and Unnikrishnan, A.S.: The monsoon currents in the north Indian Ocean, *Progr.*  
517 *Oceanogr.*, 52, 63-120, [https://doi.org/10.1016/s0079-6611\(02\)00024-1](https://doi.org/10.1016/s0079-6611(02)00024-1), 2002.

518 Stoll, H. M., Vance, D., and Arevalos, A.: Records of the Nd isotope composition of seawater from the Bay of Bengal:  
519 Implications for the impact of Northern Hemisphere cooling on ITCZ movement, *Earth Planet. Sci. Lett.*, 255, 213-  
520 228, <https://doi.org/10.1016/j.epsl.2006.12.016>, 2007.



521 Sun, Y., Clemens, S.C., Morrill, C., Lin, X., Wang, X., and An, Z.: Influence of Atlantic meridional overturning circulation  
522 on the East Asian winter monsoon, *Nat. Geosci.*, 5, 46-49. <https://doi.org/10.1038/ngeo1326>, 2011.

523 Svensson, A., Andersen, K.K., Bigler, M., Clausen, H.B., Dahl-Jensen, D., Davies, S.M., Johnsen, S.J., Muscheler, R.,  
524 Parrenin, F., Rasmussen, S.O., Röthlisberger, R., Seierstad, I., Steffensen, J.P., and Vinther, B.M.: A 60 000 year  
525 Greenland stratigraphic ice core chronology, *Clim. Past*, 4, 47-57, <https://doi.org/10.5194/cp-4-47-2008>, 2008.

526 Tan, L., Shen, C.C., Lowemark, L., Chawchai, S., Edwards, R.L., Cai, Y., Breitenbach, S.F.M., Cheng, H., Chou, Y.C.,  
527 Duerrast, H., Partin, J.W., Cai, W., Chabangborn, A., Gao, Y., Kwiecien, O., Wu, C.C., Shi, Z., Hsu, H.H., and  
528 Wohlfarth, B.: Rainfall variations in central Indo-Pacific over the past 2,700 y, *P. Nation. Acad. Sci. USA*, 116, 17201-  
529 17206, <https://doi.org/10.1073/pnas.1903167116>, 2019.

530 Thompson, W.G., and Goldstein, S.L.: A radiometric calibration of the SPECMAP timescale, *Quat. Sci. Rev.*, 25, 3207-  
531 3215, <https://doi.org/10.1016/j.quascirev.2006.02.007>, 2006.

532 Thirumalai, K., DiNezio, P.N., Tierney, J.E., Puy, M., Mohtadi, M.: An El Niño Mode in the Glacial Indian Ocean?  
533 *Paleoceanogr. Paleoclimatol.*, 34, 1316-1327, <https://doi.org/10.1029/2019pa003669>, 2019.

534 Tierney, J.E., Pausata, F.S.R., and deMenocal, P.: Deglacial Indian monsoon failure and North Atlantic stadials linked by  
535 Indian Ocean surface cooling, *Nat. Geosci.*, 9, 46-50. <https://doi.org/10.1038/ngeo2603>, 2015.

536 Tripathy, G.R., Singh, S.K., and Bhushan, R.: Sr-Nd isotope composition of the Bay of Bengal sediment: Impact of climate  
537 on erosion in the Himalaya, *Geochem. J.*, 45, 175-186, 2011.

538 Tripathy, G.R., Singh, S.K., and Ramaswamy, V.: Major and trace element geochemistry of Bay of Bengal sediments:  
539 Implications to provenances and their controlling factors, *Palaeogeogr., Palaeoclimatol., Palaeoecol.*, 397, 20-30,  
540 <https://doi.org/10.1016/j.palaeo.2013.04.012>, 2014.

541 Turner, S., and Foden, J.: U, Th and Ra disequilibria, Sr, Nd and Pb isotope and trace element variations in Sunda arc lavas:  
542 predominance of a subducted sediment component, *Contr. Mineral. Petrol.*, 142, 43-57,

543 <https://doi.org/10.1007/s004100100271>, 2001.

544 Waelbroeck, C., Labeyrie, L., Michel, E., Duplessy, J.C., McManus, J.F., Lambeck, K., Balbona, E., and  
545 Labracherie, M.: Sea-level and deep water temperature changes derived from benthic foraminifera isotopic records,  
546 *Quat. Sci. Rev.*, 21, 295-305, [https://doi.org/10.1016/s0277-3791\(01\)00101-9](https://doi.org/10.1016/s0277-3791(01)00101-9), 2002.

547 Wang, Y.V., Larsen, T., Lauterbach, S., Andersen, N., Blanz, T., Krebs-Kanzow, Gierz, P., and Schneider, R.R.: Higher sea  
548 surface temperature in the Indian Ocean during the Last Interglacial weakened the South Asian monsoon, *P. Natl.*  
549 *Acad. Sci. USA*, 119, e2107720119. <https://doi.org/10.1073/pnas.2107720119>, 2022.

550 Weber, M.E., Lantzos, H., Dekens, P., Das, S.K., Reilly, B.T., Martos, Y.M., Meyer-Jacob, C., Agrahari, S., Ekblad, A.,  
551 Titschack, J., Holmes, B., and Wolfgramm, P.: 200,000 years of monsoonal history recorded on the lower Bengal Fan  
552 - strong response to insolation forcing, *Glob. Planet. Change*, 166, 107-119,  
553 <https://doi.org/10.1016/j.gloplacha.2018.04.003>, 2018.

554 Weldeab, S., Rühlemann, C., Bookhagen, B., Pausata, F.S.R., and Perez - Lua, F.M.: Enhanced Himalayan Glacial Melting  
555 During YD and H1 Recorded in the Northern Bay of Bengal, *Geochem., Geophys., Geosy.*, 20, 2449-2461,  
556 <https://doi.org/10.1029/2018GC008065>, 2019.

557 Weldeab, S., Rühlemann, C., Ding, Q., Khon, V., Schneider, B., and Gray, W.R.: Impact of Indian Ocean surface  
558 temperature gradient reversals on the Indian Summer Monsoon, *Earth Planet. Sci. Lett.*, 578, 117327,  
559 <https://doi.org/10.1016/j.epsl.2021.117327>, 2022.

560 Winkler, A., Wolf-Welling, T., Statterger, K., and Thiede, J.: Clay mineral sedimentation in high northern latitude deep-  
561 sea basins since the Middle Miocene (ODP Leg 151, NAAG), *Internat. J. Earth Sci.*, 91 (1), 133-148,  
562 <https://doi.org/10.1007/s005310100199>, 2002.

563 Yan, Q., Owen, L.A., Zhang, Z., Jiang, N., and Zhang, R.: Deciphering the evolution and forcing mechanisms of glaciation  
564 over the Himalayan-Tibetan orogen during the past 20,000 years, *Earth Planet. Sci. Lett.*, 541, 116295,

565 <https://doi.org/10.1016/j.epsl.2020.116295>, 2020.

566 Ye, W., Liu, S., Fan, D., Zhang, H., Cao, P., Pan, H. -J., Li, J., Li, X., Fang, X., Khokiattiwong, S., Kornkanitnan, N., and  
567 Shi, X.: Evolution of sediment provenances and transport processes in the central Bay of Bengal since the Last Glacial  
568 Maximum, *Quat. Internat.*, (in press). <https://doi.org/10.1016/j.quaint.2020.12.007>, 2020.

569 Yu, Z., Colin, C., Wan, S., Saraswat, R., Song, L., Xu, Z., Clift, P., Lu, H., Lyle, M., Kulhanek, D., Hahn, A., Tiwari, M.,  
570 Mishra, R., Miska, S., and Kumar, A.: Sea level-controlled sediment transport to the eastern Arabian Sea over the past  
571 600 kyr: clay minerals and Sr-Nd isotopic evidence from IOD site U1457, *Quat. Sci. Rev.*, 205, 22-34,  
572 <https://doi.org/10.1016/j.quascirev.2018.12.006>, 2019.

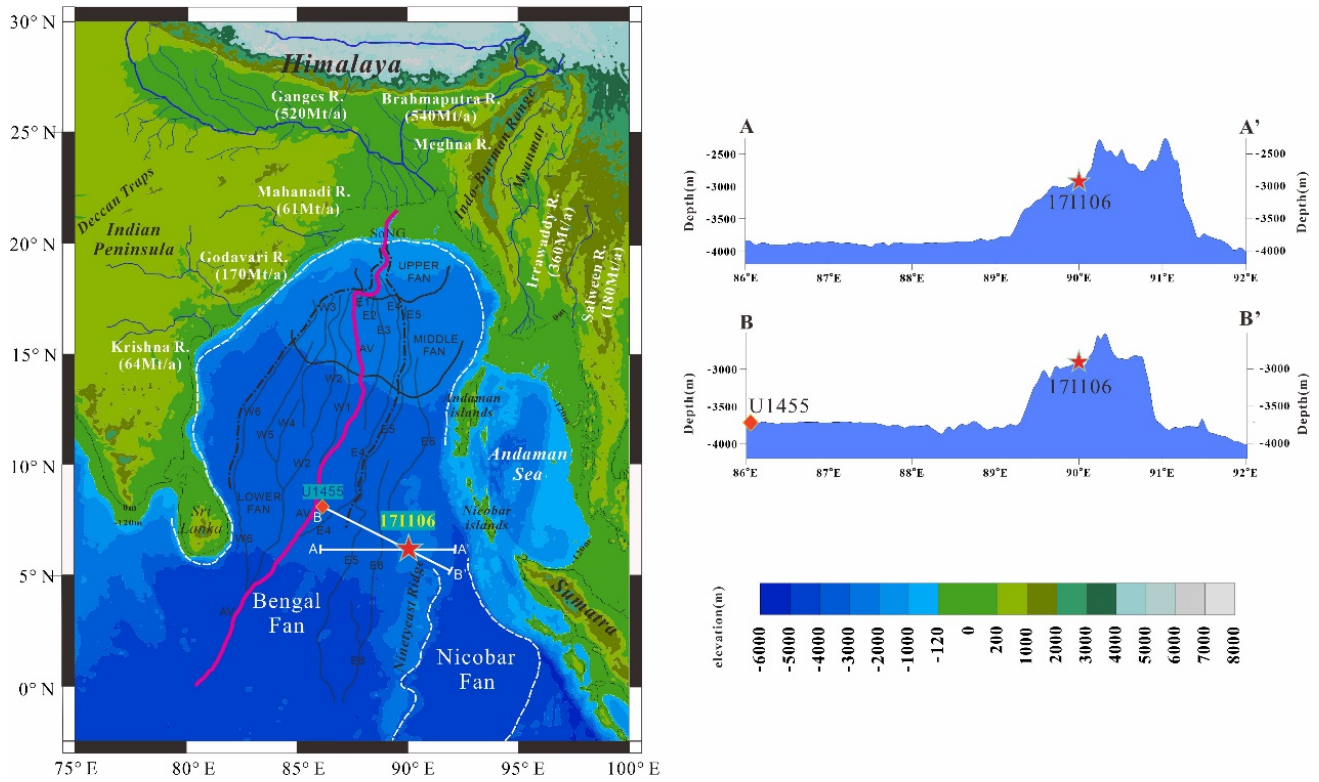
573 Zhang, E., Chang, J., Shulmeister, J., Langdon, P., Sun, W., Cao, Y., Yang, X., and Shen, J.: Summer temperature  
574 fluctuations in Southwestern China during the end of the LGM and the last deglaciation, *Earth Planet. Sci. Lett.*, 509,  
575 78-87, <https://doi.org/10.1016/j.epsl.2018.12.024>, 2019.

576 Zhang, X., Zheng, Z., Huang, K., Yang, X., and Tian, L.: Sensitivity of altitudinal vegetation in southwest China to changes  
577 in the Indian summer monsoon during the past 68000 years, *Quat. Sci. Rev.*, 239, 106359,  
578 <https://doi.org/10.1016/j.quascirev.2020.106359>, 2020.

579 Zhuravleva, A., Hüls, M., Tiedemann, R., and Bauch, H. A.: A 125-ka record of northern South American precipitation and  
580 the role of high-to-low latitude teleconnections, *Quat. Sci. Rev.*, 270, 107159,  
581 <https://doi.org/10.1016/j.quascirev.2021.107159>, 2021.

582 Zorzi, C., Sanchez Goñi, M.F., Anupama, K., Prasad, S., Hanquiez, V., Johnson, J., and Giosan, L.: Indian monsoon  
583 variations during three contrasting climatic periods: The Holocene, Heinrich Stadial 2 and the last interglacial–glacial  
584 transition, *Quat. Sci. Rev.*, 125, 50-60, <https://doi.org/10.1016/j.quascirev.2015.06.009>, 2015.

585 **Figure Captions**



586

587

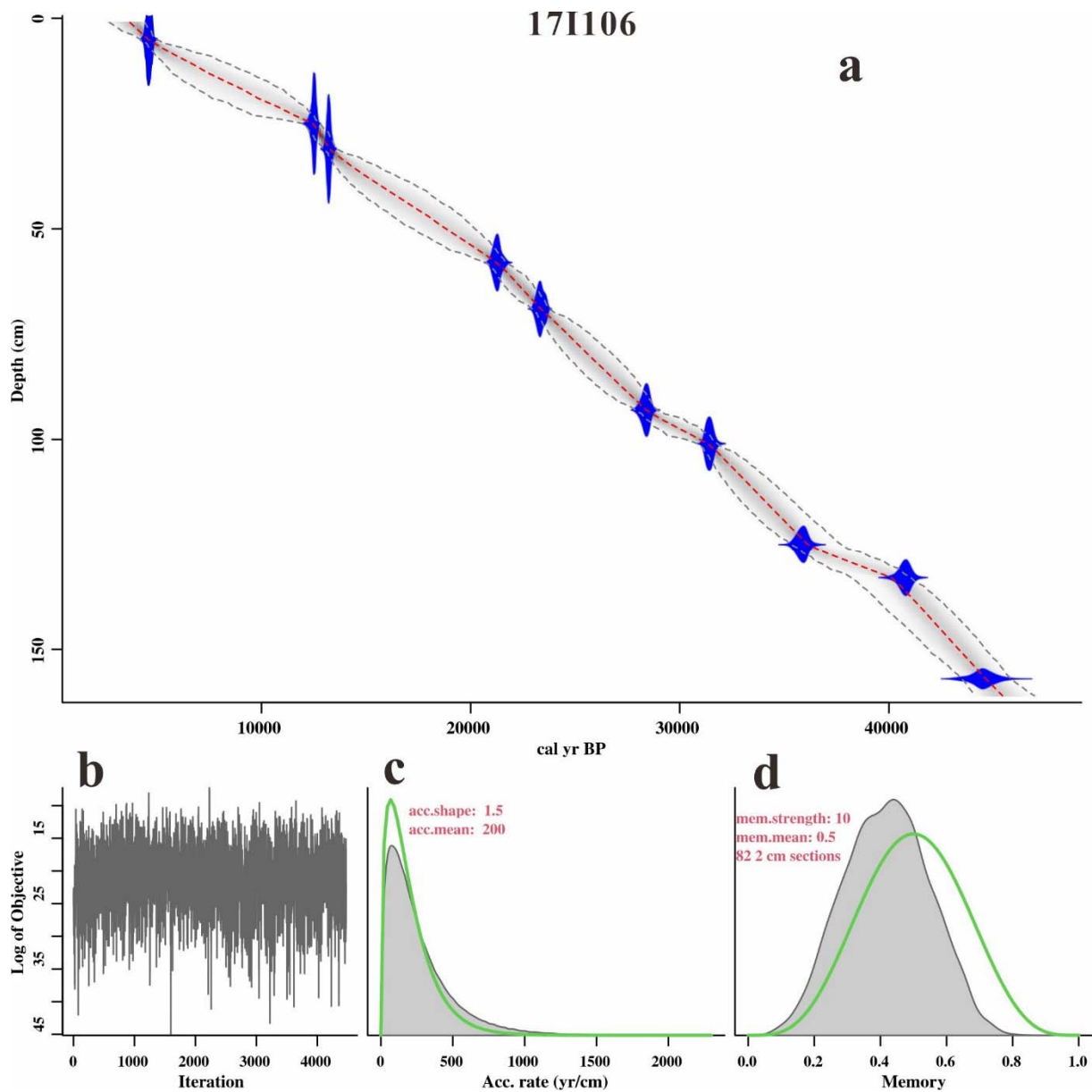
**Figure 1.** Geographical setting of the BoB. The locations of cores 171106 (red asterisks) and U1455 (orange diamond) are shown. On the left, the white dashed lines outline the scale of the Bengal Fan and the Nicobar Fan. The pink solid line is the “active” channel, and solid gray lines and black letters represent the turbidity channel and the reference names of the principal channels. The dotted-dashed line is the outline of the most recently active subfan (Curry et al., 2003). The solid white lines denote the two profile positions, which are shown on the right with the water depth legend.

588

589

590

591



592

593

594

595

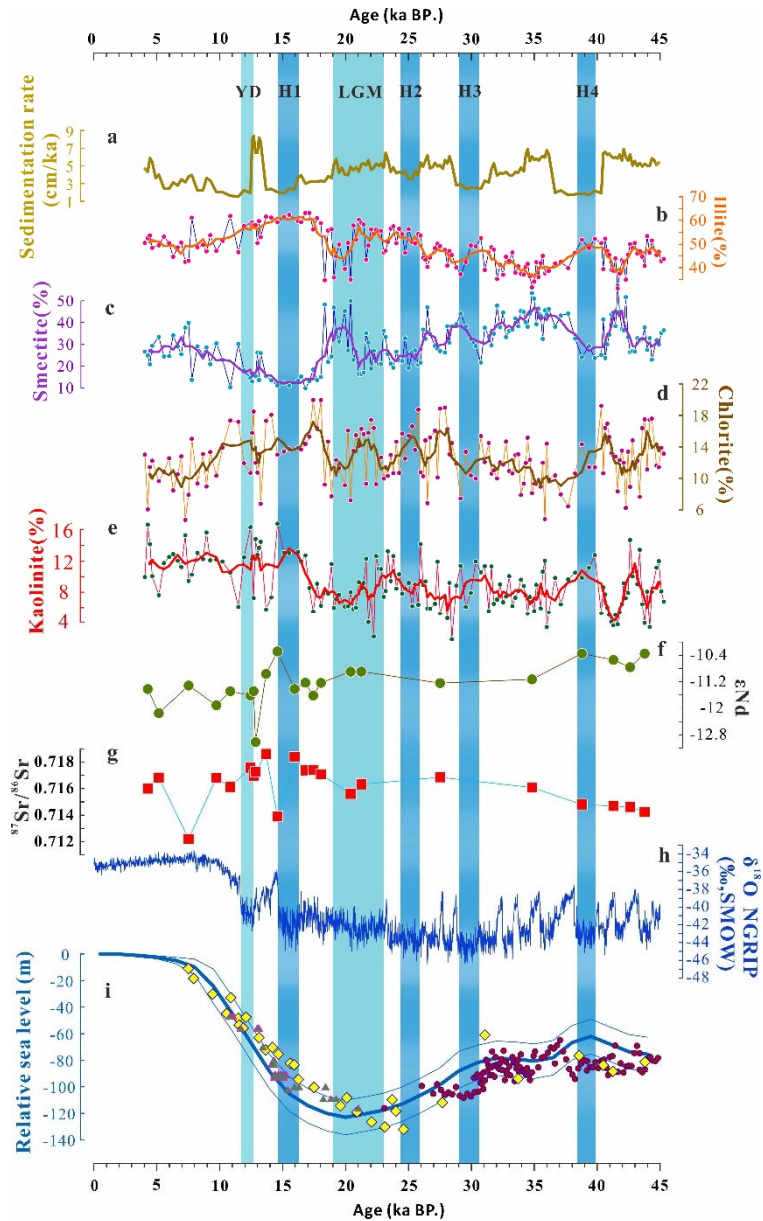
596

597

598

599

**Figure 2.** Age-depth model of core 17I106 in the northeastern Indian Ocean. **a**, Calibrated  $^{14}\text{C}$  dates (blue, with  $2\sigma$  errors) and the resulting age-depth model (the darker gray shading indicates more likely calendar ages; the gray stippled lines show 95% confidence intervals; and the red curve shows the single 'best' model based on the weighted mean age for each depth). **b**, Number of Markov chain Monte Carlo (MCMC) iterations used to generate the grayscale graphs. **c**, Prior (green) and posterior (gray) distributions of the sediment accumulation rates (the mean sediment accumulation rate was  $\sim 2$  years/cm). **d**, Prior (green) and posterior (gray) memory distributions (dependence of the sediment accumulation rate between neighboring depths).



600

601 **Figure 3.** Comparison of clay mineral and Sr-Nd isotopes data in the northeastern Indian Ocean with paleoclimate records.

602 **a,** Sedimentation rate in core 17I106; **b, c, d, e,** illite, smectite, chlorite and kaolinite percentages in core 17I106 (thick line

603 represents a 3-point running average); **f, g**  $^{87}\text{Sr}/^{86}\text{Sr}$  and  $\epsilon\text{Nd}$  values of core 17I106 in the northeastern Indian Ocean; **h,**

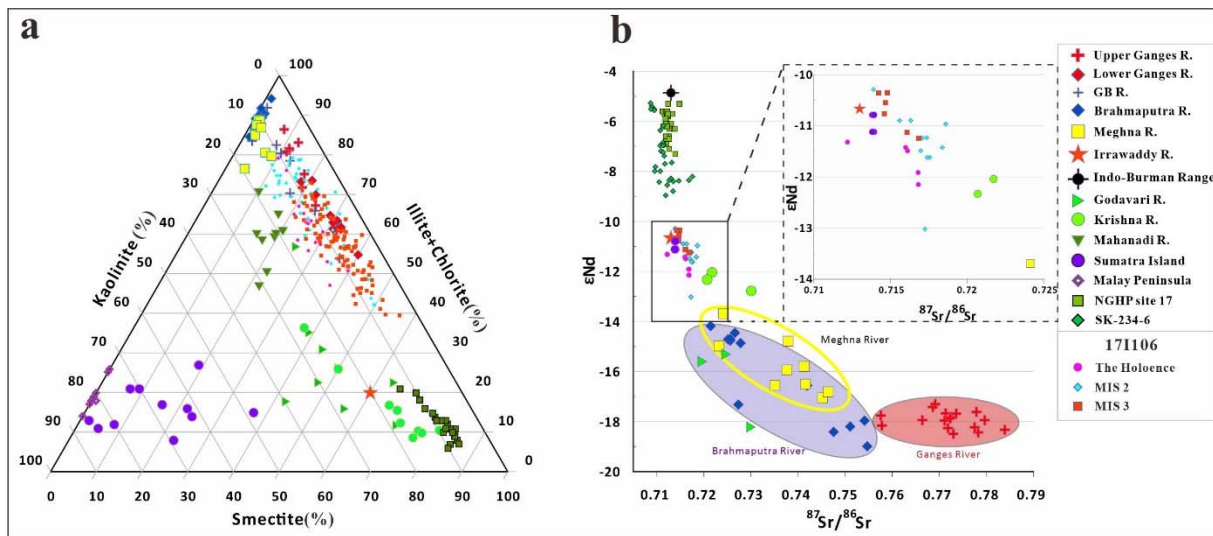
604  $\delta^{18}\text{O}$  data of Greenland ice core NGRIP (Svensson et al., 2008); **i,** Global sea level as proxy for ice volume, reconstructed

605 from benthic  $\delta^{18}\text{O}$  (thick cyan line, thin cyan line represents the 95% confidence interval, Thompson and Goldstein, 2006),

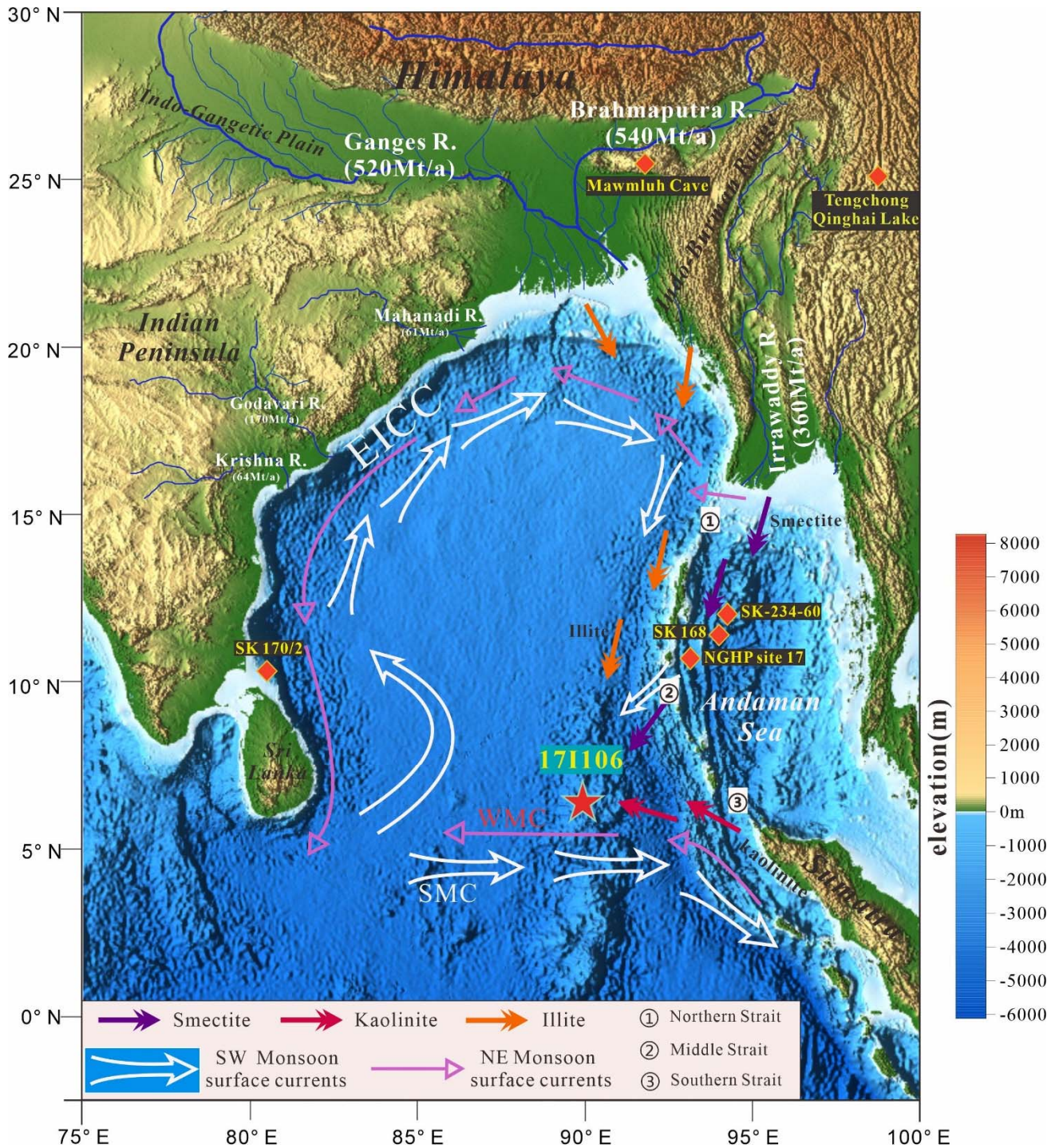
606 globally distributed corals (yellow dots, Waelbroeck et al., 2002) and sea level data (Triangles and red dots) collected by

607 Grant et al.(2014) and Hanebuth et al. (2000). Blue and cyan bars represent cold climate periods of Heinrich events (H1-

608 H4) together with Younger Dryas (YD) and the last glacial maximum (LGM), respectively.



609  
610 **Figure 4.** Sediment provenance of core 171106 in the northeastern Indian Ocean. **a**, Sediment provenance discrimination  
611 diagram in the northeastern Indian Ocean. For comparison, clay mineral data obtained from sediments collected in the  
612 modern Ganges River, Brahmaputra River Lower, Ganges-Brahmaputra River Lower and Meghna River (Khan et al., 2019),  
613 Mahanadi and Krishna Rivers of Indian Peninsula (Bejugam and Nayak, 2017), Irrawaddy River (Rodolfo, 1969), and  
614 Sumatra and Malay Peninsula rivers (Liu et al., 2012) are also plotted. The referenced cores comprise NGHP Site 17 (Ali  
615 et al., 2015), representing the Irrawaddy River as the main clay mineral source in the Andaman Sea. **b**, Variations in  $\epsilon\text{Nd}$   
616 (0) vs.  $^{87}\text{Sr}/^{86}\text{Sr}$  measured in core 171106 compared with those measured in river sediments and bulk rock samples collected  
617 around the BoB. In this diagram, we display data collected from Indian river samples (from the Godavari and Krishna  
618 Rivers) (Ahmad et al., 2009) from different parts of the modern G-B River system (Lupker et al., 2013). Measurements  
619 taken from sediments obtained from the Irrawaddy River (Colin et al., 1999), formations from the Indo-Burman ranges  
620 (Licht et al., 2013) and volcanic products of Sumatra Island (Turner et al., 2001) are also plotted. The referenced cores  
621 include NGHP Sites 17 and SK-234-60, both of which indicate that the Irrawaddy River is the main Sr-Nd isotope source  
622 for the Andaman Sea.



623

624

**Figure 5.** Map showing dispersal patterns of the BoB clay minerals for core 171106. The locations of core 171106 (red

625

asterisks) and of the reference core and sites are shown: SK 170/2 in the northern BoB, SK-168, SK-234-60, NGHP site

626

17 in the western Andaman Sea, and Mawmluh Cave in northeastern India and Tengchong Qinghai Lake in China are

627

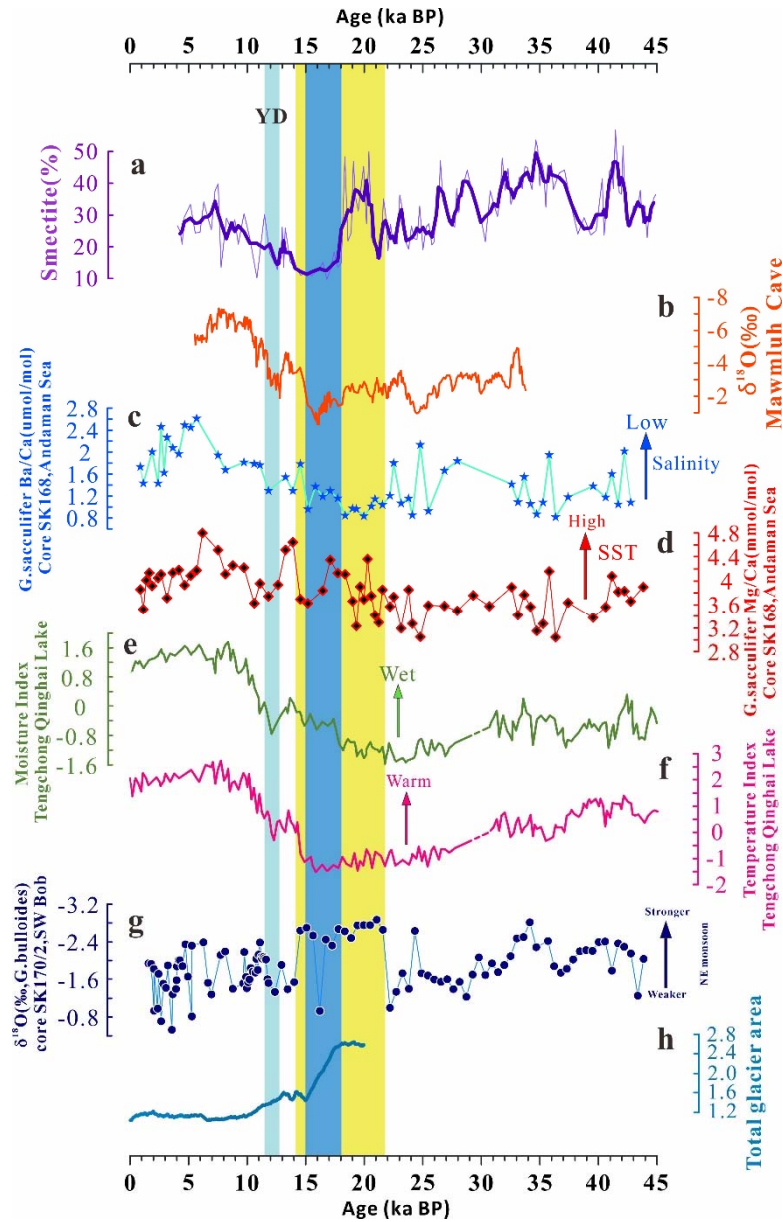
represented by orange diamonds. The orange, purple and red arrows represent the main dispersal directions of illite,

628

smectite and kaolinite when the fluvial sediments were discharged into core 171106. The white and red arrows denote the

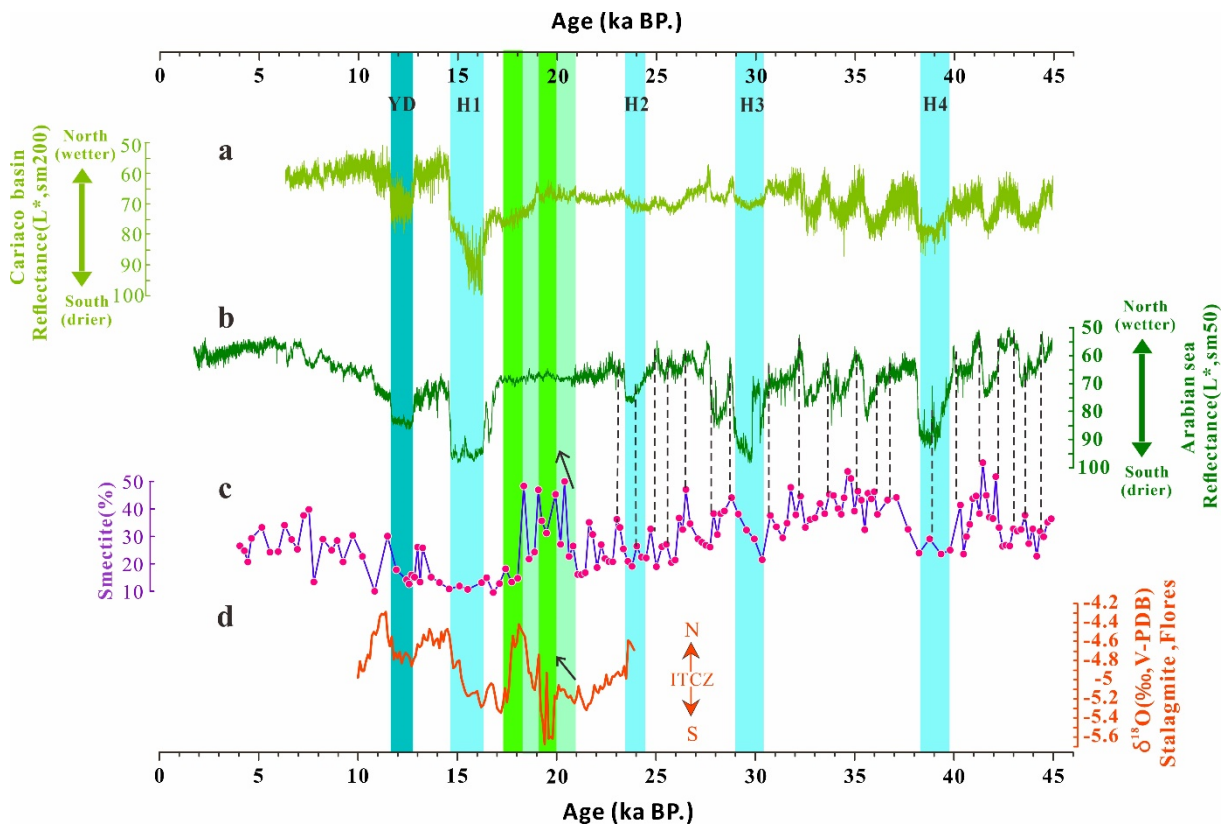


629 SW and NE monsoon currents, respectively. In the western BoB, the East Indian Coastal Current (EICC) reverses annually  
 630 with the monsoon wind (Schott and McCreary, 2001). In the lower-latitude regions of the BoB, monsoon-driven currents  
 631 flow eastward in summer to form the summer monsoon current (SMC) and westward in winter to form the winter monsoon  
 632 current (WMC) (Shankar et al., 2002). The elevation legend is shown to the right of this figure.



633  
 634 **Figure 6.** Comparison of smectite percentages in core 171106 with paleoclimate records. **a**, Smectite percentages in core  
 635 171106 (thick line represents a 3-point running average); **b**, Mawmluh Cave  $\delta^{18}\text{O}$  record for the interval 33,800 to 5500  
 636 years BP (Dutt et al., 2015). **c**, **d**, Ba/Ca and Mg/Ca of the mixed layer species *G. sacculifer* in core SK 168 from the

637 Andaman Sea, which represent the surface sea salinity and temperature, and the lower salinity and higher temperature  
 638 showed a strong SW monsoon (Gebregiorgis et al., 2016). e, f, Moisture index and temperature index from pollen records  
 639 from Tengchong Qinghai Lake, respectively (Peng et al., 2019; Zhang et al., 2020). g,  $\delta^{18}\text{O}$  variability record of planktic  
 640 foraminifera *Orbulina universa* obtained from core SK-170/2 recovered from the southwestern Bay of Bengal, which  
 641 represents the strength of the NE monsoon (Gautam et al., 2020). h, Ratio of the modeled total glacier area over the southern  
 642 parts of the Himalayan-Tibetan orogen to the present level (Yan et al., 2020). Yellow, blue and cyan bars represent the  
 643 strong NE monsoon period shown by line g, the main periods of glacier melting in the southern Himalayas shown by line  
 644 h and the cold climate periods of the Younger Dryas (YD).



645  
 646 **Figure 7.** Comparison of smectite percentages with ITCZ north-south shift records. a, L\* represents the ITCZ shift from  
 647 the Cariaco Basin (Deplazes et al., 2013); b, L\* represents the ITCZ shift from the Arabian Sea (Deplazes et al., 2013); c,  
 648 Smectite percentages in core 17I106; d, Stalagmite  $\delta^{18}\text{O}$  record from Flores (Ayliffe et al., 2013). The gold dotted line  
 649 denotes the connection between the northward movement of the ITCZ and the peak smectite percentage, and the series of

650 color bars from 21-18 ka represent the ITCZ-shift periods recorded in **d**. The green bars represent the consistent periods  
 651 shown in **c** and **d** in the late LGM, and the black arrows in **c** and **d** indicate great differences between the smectite  
 652 percentages and ITCZ record in the EIO.

653 **Table 1.** Carbon-14 and calibrated calendar ages of mixed planktonic foraminifera measured in core 17I106 in the  
 654 northeastern Indian Ocean.

Number	Depth (cm)	Materials	Measured $^{14}\text{C}$ age (yr BP, $\pm 1\sigma$ )	Calendar median age (yr BP)
1	5	mixed planktonic foraminifera	4160 $\pm$ 30	4053
2	25	mixed planktonic foraminifera	10690 $\pm$ 40	11880
34	31	mixed planktonic foraminifera	11460 $\pm$ 40	12801
4	58	mixed planktonic foraminifera	17910 $\pm$ 50	20710
5	69	mixed planktonic foraminifera	20050 $\pm$ 60	23183
6	93	mixed planktonic foraminifera	24590 $\pm$ 90	27883
7	101	mixed planktonic foraminifera	27820 $\pm$ 120	31074
8	125	mixed planktonic foraminifera	31820 $\pm$ 200	35455
9	133	mixed planktonic foraminifera	36370 $\pm$ 280	40434
10	157	mixed planktonic foraminifera	42190 $\pm$ 560	44167

655